

KLAUDIA BURKA
TOMASZ BOLD
IWONA GRABOWSKA-BOLD

COMPUTATIONAL CHALLENGES IN THE MEASUREMENT OF HEAVY-ION COLLISION EVENT CHARACTERISTICS WITH THE ATLAS EXPERIMENT AT THE LHC

Abstract *Heavy-ion collisions at extreme energies are expected to recreate conditions present in the early universe, producing a state of matter called the Quark Gluon Plasma (QGP). This state is characterized by very low viscosity resembling the properties of a perfect fluid. In such a medium, density fluctuations can easily propagate. In experimental practice, the size of these fluctuations is estimated by measuring the angular correlation of the particles produced. The aim of this paper is to present results of the measurements of the azimuthal anisotropy of charged particles produced in heavy-ion collisions with the ATLAS detector using the LHC Grid infrastructure for bulk processing of the data and resources available at the Tier-2 computing center for the final analysis stage.*

Keywords high energy physics, ATLAS experiment, heavy-ion collisions, Grid computing, statistical methods

Citation Computer Science 16 (1) 2015: 39–54

1. Introduction

The Large Hadron Collider (LHC) [6, 12] is the largest and most powerful particle accelerator built thus far. It is situated at the European Organization for Nuclear Research (CERN). LHC experiments have been collecting data since the fall of 2009. Most of the experimental time at the LHC is dedicated to proton-proton physics at a center-of-mass energy of 7 TeV for data collected in 2011 (and 8 TeV in 2012). However, part of the collision time is also devoted to heavy-ion (HI) physics, when lead ions are collided. There are four main experiments collecting collision data at the LHC. One of them is ATLAS [2]. For a recent review of ATLAS results, see [10, 19]. In the domain of HI physics, the research program of the experiment aims to elucidate the properties of the QGP [28].

The ATLAS electronic readout consists of several million channels. With a collision frequency of 20 MHz in 2011/12, the raw-data rate out of the detector surpassed 0.5 PB/s. The physics processes of interest are less frequent, and the initial rate is reduced to interesting collisions only by the three-staged trigger system. The first level is built with custom electronics implementing a hard-real-time system capable of taking the decision within $2.5 \mu\text{s}$ while reducing the rate of accepted events to about 100 kHz. Further, rate reduction is achieved with an additional two levels of the trigger system. It is implemented as a farm of 15k cores of commodity computers and reduces the rate of accepted events to about ~ 400 Hz performing finer filtering of the incoming data [3]. The data rate to disk reaches about 700 MB/s. The raw data is promptly reconstructed at Tier-0 located at CERN, and derived formats are distributed to Grid sites for analysis.

In ultra-relativistic HI collisions at sufficiently high energy densities, quarks and gluons become deconfined. In nature, such systems might exist inside neutron stars or collapsing supernovae. The ones created in the HI collisions are comparatively small in volume and short lived. Nonetheless, the controlled environment of the experiment allows for precise studies of the properties of such a system. The unexpected result of the early experiments was the discovery that matter created in HI collisions does not resemble a gas (as earlier predicted), but exhibits features of a fluid. The properties of this fluid were also found to be unusual. The QGP behaves similar to a perfect fluid with extremely low viscosity. Its properties are well described by hydrodynamics assuming very low values of shear viscosity (lower than that of super-fluid ^3He) [14, 7, 26]. As a consequence, initial anisotropies of density propagate through the system. One of the phenomena in such a system is a collective flow in which the initial spatial anisotropy of the collision zone is transformed into a final state momentum anisotropy. The flow phenomenon is studied due to its sensitivity to the early stages of the collision system and its hydrodynamical evolution [23]. At the LHC, the HI collision energy in Run I (2010–2011) was 2.76 TeV per nucleon pair. It is more than a factor 10 higher than at RHIC. As a consequence, the greater volume of a high-temperature QGP is produced in Pb+Pb collisions at the LHC (as compared to HI collisions at RHIC). Together with the higher luminosities and excellent

detectors, this flow phenomenon can be studied in more detail. Experimentally, the flow manifests itself as a significant anisotropy of the particle momenta in a plane perpendicular to beam direction. Azimuthal flow is commonly characterized by coefficients, v_n , of the Fourier expansion of the particle azimuthal angle distributions [30]. The most extensively-studied coefficient is the second harmonic, v_2 , which predominantly originates from the elliptical shape of the collision zone in non-central HI collisions. The v_2 in central collisions and higher harmonics are sensitive to the initial spatial fluctuations of interacting nuclei, and their non-vanishing values up to v_6 are observed.

In this paper, the measurements of the second harmonic (v_2) of the Fourier decomposition of the charged particles in lead-lead (Pb+Pb) collisions with the ATLAS detector at the LHC are presented. There are a number of techniques that are used for flow measurements; however, the simplest yet most robust are favored. The study is focused on validating a superior newer technique as comparison to previously-established measurements [9, 4].

2. Grid computing for ATLAS experiment

The ATLAS detector [2] provides nearly full solid-angle coverage around the interaction point (IP) with tracking detectors, calorimeters and muon chambers, which are well suited for measurements of correlations over a large pseudorapidity range.

In ATLAS, at least one collision takes place every 50 ns; i.e., with a frequency of 20 MHz (Run I). The trigger output rate has increased over the years to ~ 400 Hz in 2012, giving more than 5.5×10^9 recorded physics collisions. In 2010, experiments at the LHC produced their nominal 15 PB of data per year. Since then, they have increased to 23 PB in 2011 and 27 PB in 2012. About 10% of that volume is used by the Pb+Pb and p+Pb data set.

Due to the large amount of data, the ATLAS computing model embraces the Grid paradigm as well as a high degree of decentralization and sharing of computing resources. The required amount of computing resources is vital to the operation of ATLAS in a way that was not the case for previous CERN-based experiments.

The primary event processing occurs at CERN in a Tier-0 facility shared among LHC experiments. It has a capacity of about 68 000 cores, which is about a third of the LHC computing Grid total capacity of approximately 235 000 cores. Tier-0 is linked with the Tier-1 centers (which are typically regional research institutes), and each is connected with a series of Tier-2 computer centers (mostly situated in universities). The bandwidth used by LHC experiments is impressive: 1.5–2 GB/s flow continuously from CERN to the Tier-1 centers, and the worldwide flow of LHC-related data is 7.5–10 GB/s.

The process of handling particle physics data can be broken down into four main parts, as sketched in Figure 1. First, the raw detector data is filtered and stored for reconstruction. In the case of Monte Carlo (MC) simulations, the first step is replaced by event generation and detector-response simulation, which are the most

CPU-intensive parts. Data from both the MC and detector simulations are then reconstructed by the same reconstruction programs.

The final stage is the analysis itself. Figure 2 shows the number of completed tasks in the Grid per day in the ATLAS experiment in 2012. The tasks are broken up into various categories, with MC production and user analyses being the top consumers. A smaller fraction of jobs are needed for specific MC group productions as well as analyses performed by a group rather than a single analyzer. A fraction of the time is also used for validation of new MC simulations and Grid infrastructure testing.

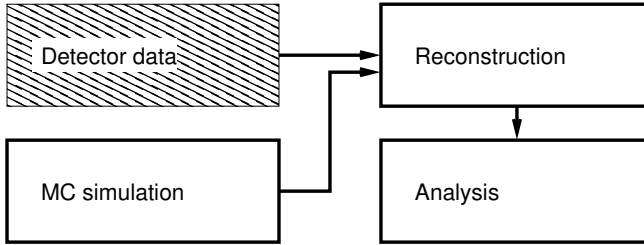


Figure 1. Schematic view of the main LHC data processing stages. The shaded box represents the detector data for which virtually no processing is needed, while hollow boxes represent a stage of processing on the Grid.

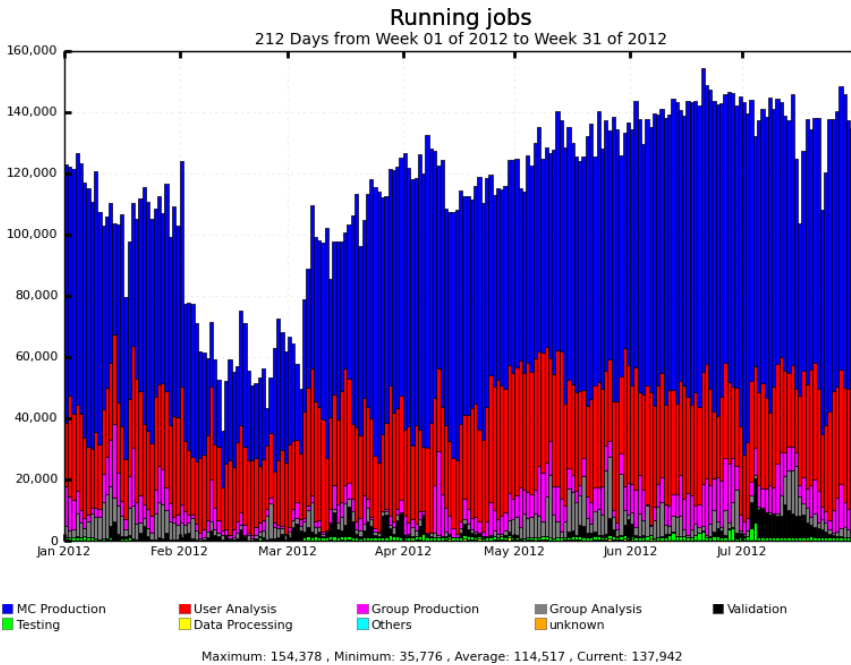


Figure 2. Number of completed tasks in the Grid per day in the ATLAS experiment in 2012.

2.1. Grid computing in Poland

In Poland, the ATLAS experiment is supported by two computing centers: Academic Computing Center CYFRONET AGH in Krakow, and Supercomputing and Networking Center in Poznan. Both are members of the Polish Tier-2 organization. Within this support, ATLAS software is provided and computational resources are granted.

Among Polish sites, CYFRONET is the largest, with a dedicated support for ATLAS users. One of the CYFRONET supercomputers is ZEUS which has 25468 cores, a computational power of 374 TFLOPS, 60 TB of RAM, and disk storage with a capacity of 2.3 PB. As of this writing (2014), this is currently the most powerful computer cluster in Poland. For more information, see [1]. ZEUS can perform ~ 8 million computing tasks per year. This can considerably reduce the computation time and allow for analysis of large-scale scientific problems. The ZEUS cluster has been used to obtain the results presented in this paper.

3. The HI collisions

Several stages in HI collisions can be distinguished. At the initial stage (before the actual collision), two nuclei are brought to collision at a speed close to the speed of light, which results in the Lorentz contraction of the nuclei along the direction of flight. Since the nuclei's transversal dimensions are not affected, collisions with various degrees of overlap can occur. The degree of overlap can be described by means of the impact parameter, defined as the distance between the centers of the two colliding nuclei. Collisions with an impact parameter near zero are called central, while collisions with an impact parameter approaching 2 times the radius of the nuclei are called peripheral. In peripheral collisions, only a small fraction of nucleons participate in the collisions. The nucleons outside the overlap region (called spectators) travel almost intact along the beam direction.

In the early stages of the collision, hard scatterings take place. A large amount of energy is deposited in a small region of space and in a short duration of time. Matter in the collision zone has very high energy density and temperature, which could be sufficient to reach the phase-transition condition. The huge pressure gradient inside the interaction region leads to a rapid expansion of the system. The QGP cools down, and the quarks and gluons combine back into hadrons (this process is thus called hadronization). The particles produced are then measured by the detector.

4. Elliptic flow

It is observed that particles produced in non-central collisions are emitted in the direction of the reaction plane, which is defined by beam direction (z-axis) and impact parameter (see Fig. 3). A region where the QGP is produced (the so-called "fireball") has an elliptical shape caused by the initial spatial anisotropy of the collision. This shape anisotropy gives rise to a pressure gradient that is stronger in the direction of the reaction plane; finally, this leads to a momentum anisotropy in the final state.

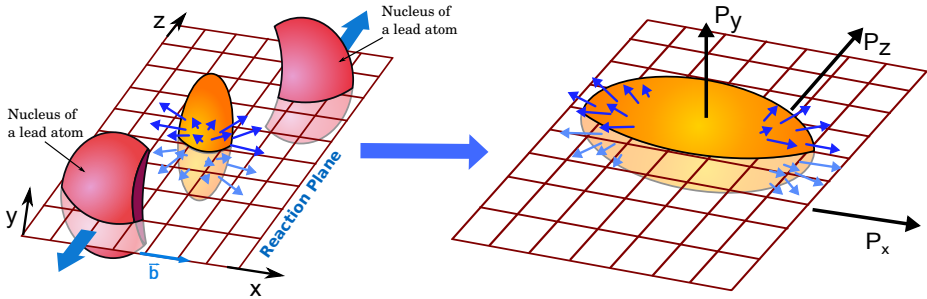


Figure 3. Sketch of the HI non-central collision and expansion of the resulting fireball. An orange almond-shaped region denotes the collision zone (left) and hydrodynamically expanded plasma (right), while the pink shapes represent spectators. The reaction plane is represented as a mesh. The coordinate system is chosen so that the impact parameter is in the x direction of the system and z is along the initial direction of the nucleons.

Customarily, the produced particle distribution measured with respect to the reaction plane is expanded in a Fourier series [29, 16]:

$$\frac{2\pi}{N} \frac{dN}{d\phi} = 1 + \sum_{n=1}^{\infty} 2v_n \cos[n(\phi - \Phi_n)] = \sum_{n=-\infty}^{\infty} v_n e^{in\Phi_n} e^{-in\phi}, \quad (1)$$

where ϕ is the azimuthal angle of a charged particle, v_n is the amplitude of anisotropic flow in the n -th harmonic, and Φ_n is the corresponding symmetry angle. The v_n amplitudes can be calculated as:

$$v_n = \langle \cos[n(\phi_i - \Phi_n)] \rangle, \quad (2)$$

where the angle brackets denote an average over all particles in all events. The v_n coefficients are functions of rapidity and transverse momentum. The sine terms are negligible. The first harmonic, v_1 , called *directed flow*, describes the sideward motion of fragments in ultra-relativistic nuclear collisions, and it carries early information from the collision. The second harmonic, *elliptic flow* – v_2 , measures the elliptical shape of the distribution of the particles' momenta in the transverse plane. The higher-order coefficients (v_3 – *triangular flow*, v_4 – *quadrangular flow* etc.) are important, as they provide insight into the initial-state geometric fluctuations which arise from fluctuations in the initial position of the nucleons within the nuclei. The Fourier v_n coefficients are measured to be non-zero up to 6-th mode, which itself is the indication of the very low shear viscosity to entropy ratio of the QGP medium [21, 24, 22].

Centrality of the HI collision is defined in ATLAS using the total transverse energy in the Forward Calorimeter (FCal) ($3.2 < |\eta| < 4.9$) [9]. All collision events are divided into percentile intervals based on their FCal ΣE_T values.

The most-central interval studied here (1–10%) corresponds to events with the largest FCal energy and, therefore, the smallest impact parameter. The reaction

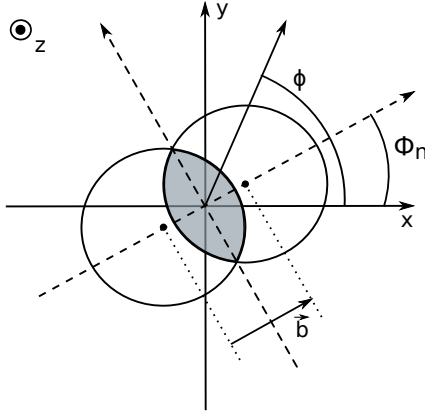


Figure 4. Transverse view of a non-central HI collision. An overlap region is marked by a shaded area. The azimuthal angle ϕ of an example particle produced in such a collision, the impact parameter \mathbf{b} and the reaction plane angle Φ_n are shown. Nuclei move along the z axis [11].

plane angle, Φ_n , as shown in Figure 4, is the angle between the reaction plane and the laboratory frame. The Φ_n can not be directly measured, but its estimate, event plane angle, Ψ_n , can be calculated from the particle azimuthal distribution for every event. The flow coefficients can be measured by the particle azimuthal correlations with Ψ_n [20].

5. Event Plane and Scalar Product

Several techniques are used to measure azimuthal anisotropies. In this paper, the standard event plane method (denoted EP) and the scalar product method (denoted SP) are compared. The event flow vector, \vec{Q}_n , is defined as $\vec{Q}_n \equiv (|Q_n| \cos(n\Psi_n), |Q_n| \sin(n\Psi_n))$ for each harmonic. For a given set of N particles belonging to the same event, the flow vector can be written as [16]:

$$Q_n = |Q_n| e^{in\Psi_n} \equiv \frac{1}{N} \sum_j e^{in\phi_j}, \quad (3)$$

where the sum goes over all particles in the considered set of particles and ϕ_j is the azimuthal angle of the particle. The Q_1 describes the average angle of the particles in the event. The event plane angle is the azimuthal angle of Q_n , denoted as:

$$\Psi_n = \frac{1}{n} \operatorname{arctg} \left(\frac{Q_y}{Q_x} \right). \quad (4)$$

where Q_x and Q_y are projections of the Q vector onto the laboratory frame axes. The Q_n vectors can be measured in regions of phase space (sub-events), which is exploited in order to obtain v_n coefficients and correct for the limited resolution of measured Ψ_n .

The correction to the measurement has to be applied, as the number of particles is limited; therefore, statistical fluctuations cause the measured reaction plane angle Φ_n to differ from Ψ_n . The measurement is corrected as follows:

$$v_n = \frac{v_n^{\text{obs}}}{R}, \quad (5)$$

where R is event plane resolution correction. The R coefficient is a function of centrality and is different for each harmonic n . To find the R experimentally, one has to divide particles from each event into independent "sub-events" (in this application, two sub-events are used). The Q_n vectors are measured in regions of the detector, and R can be obtained as:

$$R = \left\langle Q_n^A Q_n^{B*} / |Q_n^A| |Q_n^B| \right\rangle^{1/2} = \sqrt{\langle \cos(n[\Psi_n^A - \Psi_n^B]) \rangle}, \quad (6)$$

where Q_n^A , Ψ_n^A and Q_n^B , Ψ_n^B are the Q vectors and event plane angles estimated in the reference detectors (FCals) located symmetrically in forward (side A) and backward (side B) ATLAS detector regions. Due to the oddness of the sine function, the imaginary part of the resolution is vanishing.

The n -th Fourier harmonic in the EP method is defined as follows [17]:

$$v_n^{\text{EP}} = \frac{\left\langle Q_n \frac{Q_n^{A*}}{|Q_n^A|} \right\rangle}{R}. \quad (7)$$

It is obtained as a function of centrality, pseudorapidity, η , and transverse momentum, p_T and averaged over all events.

Besides the correlations between the particles induced by the genuine flow phenomena, there are also other sources of possible correlations. They are usually referred to as non-flow, and examples are the correlation of particles within the jets and resonance decays. They are characterized by a shorter (in pseudorapidity) correlation range. Therefore, in order to suppress the non-flow correlations, the separation in pseudorapidity has to be assured. This is the flow vector, Q_n , in the detector of interest, here the Inner Detector (ID) [2] is correlated with the flow vector in the reference, Q_n^A , FCal at the opposite η side of the detector, allowing the pseudorapidity separation of 3.2 units at minimum in ATLAS experimental conditions.

It has been recently discovered that the underlying v_n is not a unique function of centrality; conversely, it fluctuates from event to event [15]. In this case, the v_n^{EP} method is biased in the experiment-dependent fashion. It actually does not estimate the mean value of true v_n but some other quantity in between $\langle v_n \rangle$ and $\sqrt{\langle v_n^2 \rangle}$. Such a property of the observable makes comparisons between the experiments a harder task, as it requires that the resolution corrections have the same magnitudes. This, in turn, is only possible if the same detectors and phase space are used to obtain Q_n^A and Q_n^B . For this reason, an alternative method, Scalar Product (SP), has been proposed [27] (see discussion in [17]). In this method, detector bias is eliminated, and

the measured quantity is always the $\sqrt{\langle v_n^2 \rangle}$. Its application is very similar to the EP, as the Q vectors have to be found in the same way as in the EP method. But they are combined in order to obtain the flow amplitude:

$$v_n^{\text{SP}} = \frac{\langle Q_n Q_n^{A*} \rangle}{\sqrt{\langle Q_n^A Q_n^{B*} \rangle}}. \quad (8)$$

The elliptic flow estimated with the SP method is expected to differ by a small percentage of the measurements obtained with the EP method. For higher harmonics, this difference is supposed to be larger due to fluctuations [17].

6. Implementation

The data collected by the ATLAS experiment is divided into so-called *runs*. Customarily, one run stands for the period in which the collisions were stable at the nominal collision energy. The analysis starts with the event selection (see Fig. 5a). The criteria applied in this analysis are: the confirmation of the collision and at least one reconstructed primary vertex. In the next analysis steps, additional fine-tuning of the event selection is added. This step of the analysis is performed on the Grid, as the data volume disallows for the processing at Tier-2. The task is divided into a number of jobs by the ATLAS custom job submission system [18] and executed in parallel at many Grid sites. Therefore, the output data is stored at multiple sites.

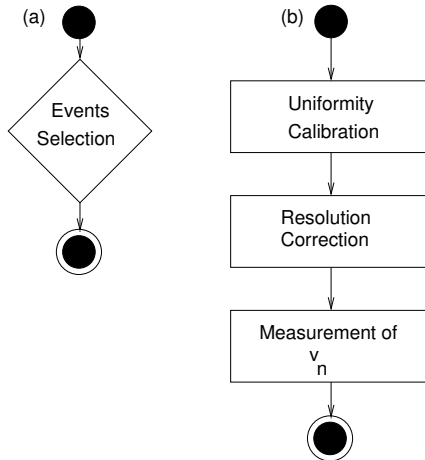


Figure 5. Schematic view of the analysis procedure: (a) the event selection step yielding the reduced data set, (b) the steps of the analysis procedure resulting the elliptic flow measurement.

The analysis data format is ROOT [5] TTree containing reconstructed physical quantities. Data analyses involve several cycles of input-file scanning to extract

the relevant information (to be described later). In order to accelerate the analysis loop, these formats are further slimmed down by removing quantities and collision events of no interest for a given analysis. After the slimming down, data volume is about 50 TB. If a final size of the data set can be reduced to a few TB, then the data can be stored in Tier-2 computing centers and processed using a local-batch system, allowing for a shorter analysis cycle. This is the case for the analysis presented here. A portion of ~ 4 TB was analyzed frequently, while processing of the entire data set involving submission to the Grid was performed only a few times. Specifically, the analysis presented in this paper has been done on one run of Pb+Pb collisions at 2.76 TeV recorded in November 2010. The data is stored at the CYFRONET computer center. In this run, about 6.5 million collision events were recorded; however, only about 3 million pass the event selection, which amounts to aforementioned ~ 4 TB of data. This data set consists of 1600 files, each containing about $2 \cdot 10^3$ events.

The time needed to perform the v_2 calculation step on this amount of data sequentially is about 160 h. Hence, the processing is divided into about 400 smaller *jobs* with only a few input files in each of them, and sent simultaneously to the queue on the ZEUS cluster as an *array job*. This approach reduces the whole processing time to about 2 hours, thus allowing for a significantly-faster turnaround of the analysis process.

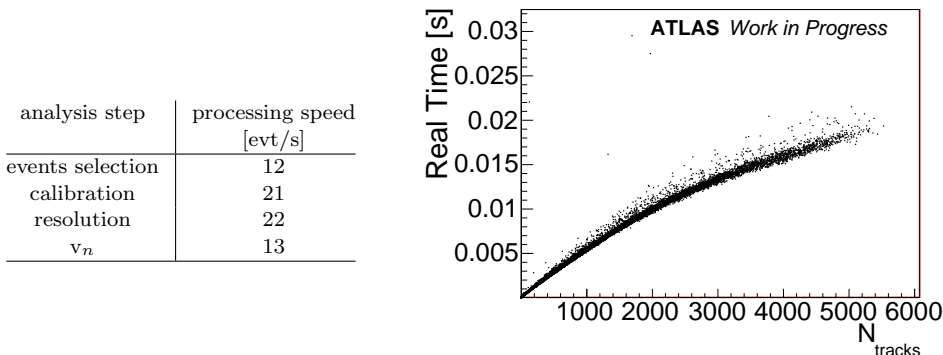


Figure 6. Event processing rate in the analysis steps (left table) and processing time per event of the last stage of the v_2 calculation as a function of the number of tracks (right plot).

Each event is composed of about 1500 tracks on average, which are built from hits deposited by charged particles in the ID. To clean up the sample from the so-called *fake tracks* which were reconstructed from random hits, some track-quality requirements also need to be imposed. They include criteria on a number of hits in the particular ID layers, the transverse momentum $0.5 < p_T < 12$ GeV, pseudorapidity $|\eta| < 1.0$, and a requirement of the track proximity to the interaction vertex. Both event and track selections are discussed in detail in [4].

After all selections are done, the methods of elliptic flow measurements are implemented as shown in Figure 5b. The first analysis step is the calculation of corrections for non-uniform detector acceptances. They are based on the assumption that there should be statistically no preferred direction of physics processes. This step is fairly simple and performed once per given data set; thus, only a small amount of processing time is consumed. In the next step, resolution correction is calculated. The first loop goes over the sub-events which correspond to the A and B sides of the reference detector. For each event, the complex vectors, Q_n^A and Q_n^B , are found and then correlated with each other (to measure the denominator of Eqs. 7 and 8). This step is computationally more expensive; but on the other hand, it needs to be computed only once for a given event selection and then reused in the following analysis.

In the next step, the actual calculation of the v_2 is performed. The loops run over the tracks in the ID. For each ϕ angle of the track, in a given pseudorapidity range, flow vector Q_n is correlated with Q_n^A or Q_n^B in order to estimate the numerator of Eqs. 7 and 8. Finally, the obtained v_2 is averaged over the events in a given centrality interval, transverse momentum, p_T , and pseudorapidity, $|\eta|$. This step is the most expensive computationally and is repeated several times in the analysis-code development and later for the estimation of systematic effects. Therefore, it dominates the overall processing time required for the analysis, as summarized in Figure 6. Processing time grows with the number of charged particle tracks analyzed per event, as also shown in Figure 6. In all stages, the throughput is partially determined by the data access that can be estimated from the throughput value of the relatively-trivial-events selection step. In this step, the computation related to the selection is minimal while the even data needs to be read in and a fraction of it written out.

7. Results

The resolution corrections for both methods were determined from the FCal in the pseudorapidity range $3.2 < |\eta| < 4.8$ and are shown in Figure 7 (left). The 1% of the most central collisions (which corresponds to FCal $\Sigma E_T > 3.46$ TeV) are excluded from the analysis due to the imprecision in the estimation of the resolution correction. For 30% of the most peripheral collisions (FCal $\Sigma E_T < 0.11$ TeV), resolution corrections drop to very low values; for this reason, these events are also not considered.

Figure 7 (right) shows the v_2 dependence on p_T in one centrality bin (30–40%) for charged particles with $|\eta| < 1$ measured with the two methods. For all centrality intervals a similar behavior is observed. There is a rapid increase of $v_n(p_T)$ up to 3 GeV, followed by a gradual fall to p_T around 7–8 GeV, and a weak p_T -dependence above ~ 9 GeV. In the low p_T region (up to 2 GeV) the elliptic flow increases almost linearly with p_T . This phenomenon is well described by hydrodynamics [13, 25, 8]. The strongest elliptic flow is observed in centralities 30–50%, due to the high initial asymmetries in the collision shape. The values of v_2 obtained from the SP method are systematically larger by about 2% than those obtained from the EP method in a majority of centrality intervals, as shown in Figure 8.

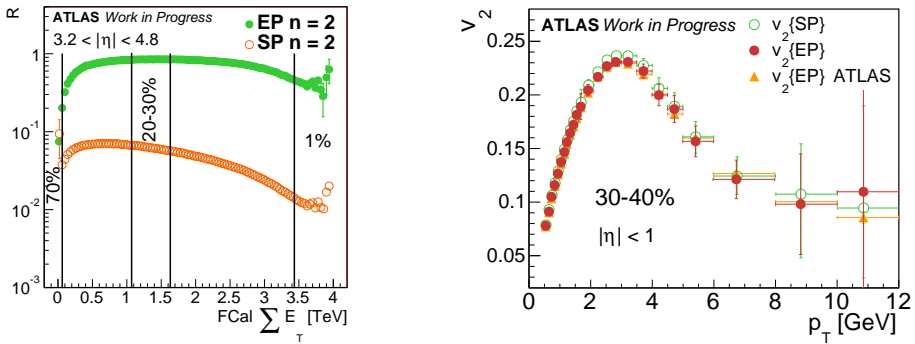


Figure 7. (left) Resolution correction as a function of FCal ΣE_T for EP (full points) and SP (open dots) methods. (right) Elliptic flow measured using the EP and SP methods in centrality bin 30–40% for p_T ranging from 0.5–12 GeV, and in the pseudorapidity interval $|\eta| < 1$. The v_2 {EP} ATLAS points come from [9].

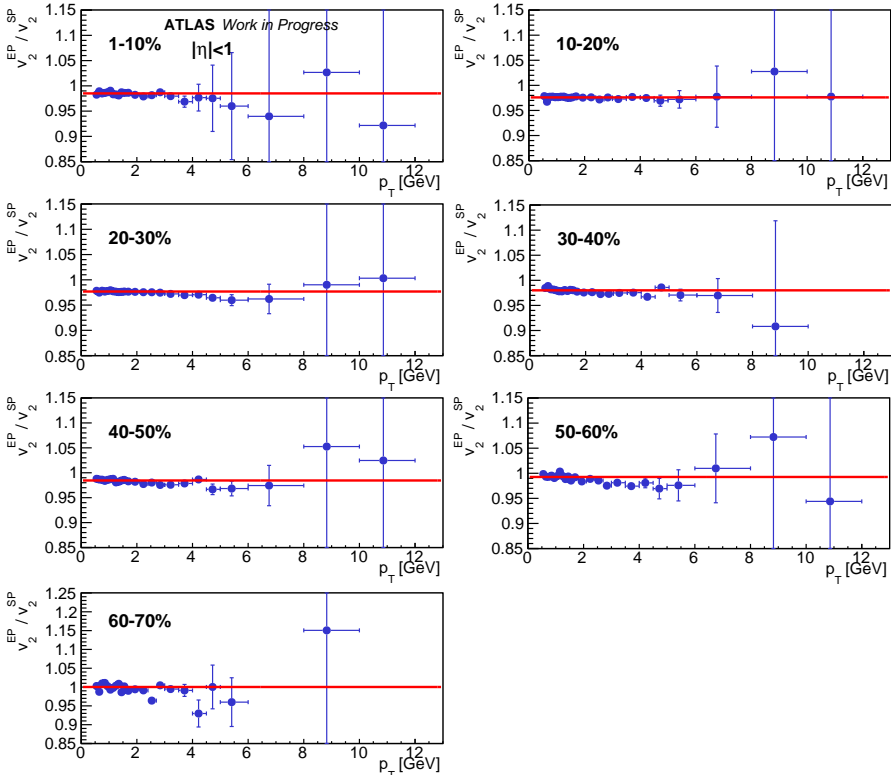


Figure 8. Ratios of elliptic flow coefficients, v_2^{EP}/v_2^{SP} , measured with the EP and SP methods as a function of p_T in different centrality classes. A constant (red line) is a fit to the points.

8. Conclusions

The second Fourier harmonic, v_2 , has been measured with the EP and SP methods in the ATLAS experiment in Pb+Pb collisions at $\sqrt{s_{NN}} = 2.76$ TeV using tracks of charged particles in the pseudorapidity range of $|\eta| < 1$ and transverse momentum p_T from 0.5 to 12 GeV. The similar p_T dependence for both methods is found in the centrality range of 1–70%. It has been demonstrated that the SP method gives systematically higher values of v_2 in comparison to the EP method, which is consistent with the predictions from [17].

Analysis of the enormous amount of data collected by the ATLAS experiment has only been possible due to the excellent Grid performance. However, in routine data analysis, a fast turnaround is essential. Therefore, data analysis on a fraction of the available data is performed in rapidly-available resources of Tier-2. The presented analysis is an example of such an arrangement where a significant reduction in analysis time was possible. This has been made possible thanks to the Tier-2 infrastructure available at CYFRONET.

Acknowledgements

The authors would like to thank the ATLAS Collaboration for providing data for this analysis and ACK CYFRONET AGH for giving us the opportunity to present our work at the KU KDM14 conference. We would like to thank the Faculty of Physics and Applied Computer Science, AGH UST for financial support. This work was supported in part by the National Science Center grant No. DEC-2011/03/B/ST2/02631. This research was supported in part by PL-Grid Infrastructure.

References

- [1] ACK Cyfronet AGH. <http://www.cyfronet.krakow.pl/>.
- [2] ATLAS Collaboration: The ATLAS Experiment at the CERN Large Hadron Collider. *JINST*, vol. 3, p. S08003, 2008. <http://dx.doi.org/10.1088/1748-0221/3/08/S08003>.
- [3] ATLAS Collaboration: Performance of the ATLAS Trigger System in 2010. *Eur. Phys. J.*, vol. C72, p. 1849, 2012. <http://dx.doi.org/10.1140/epjc/s10052-011-1849-1>.
- [4] ATLAS Collaboration: Measurement of the centrality and pseudorapidity dependence of the integrated elliptic flow in lead-lead collisions at $\sqrt{s_{NN}} = 2.76$ TeV with the ATLAS detector. *Eur. Phys. J.*, vol. C74(8), p. 2982, 2014. <http://dx.doi.org/10.1140/epjc/s10052-014-2982-4>.
- [5] Brun R., Rademakers F.: *ROOT* an object oriented data analysis framework. *Nuclear Instruments and Methods in Physics Research Section A: Accelerators, Spectrometers, Detectors and Associated Equipment*, vol. 389(12), pp. 81–86, 1997. ISSN 0168-9002. New Computing Techniques in Physics Research V. [http://dx.doi.org/http://dx.doi.org/10.1016/S0168-9002\(97\)00048-X](http://dx.doi.org/http://dx.doi.org/10.1016/S0168-9002(97)00048-X).

- [6] Brüning O. S., Collier P., Lebrun P., Meyers S., Ostojic R., Poole J., Proudlock P.: *LHC Design Report*. CERN, Geneva, 2004.
- [7] Chaudhuri A. K.: Dissipative hydrodynamics and heavy-ion collisions. *Journal of Physics G: Nuclear and Particle Physics*, vol. 35(10), p. 104015, 2008. <http://stacks.iop.org/0954-3899/35/i=10/a=104015>.
- [8] ALICE Collaboration: Elliptic flow of charged particles in Pb-Pb collisions at 2.76 TeV. *Phys. Rev. Lett.*, vol. 105, p. 252302, 2010. <http://dx.doi.org/10.1103/PhysRevLett.105.252302>.
- [9] ATLAS Collaboration: Measurement of the pseudorapidity and transverse momentum dependence of the elliptic flow of charged particles in lead-lead collisions at $\sqrt{s_{NN}} = 2.76$ TeV with the ATLAS detector. *Phys. Lett.*, vol. B707, pp. 330–348, 2012. <http://dx.doi.org/10.1016/j.physletb.2011.12.056>.
- [10] ATLAS Collaboration: Observation of a new particle in the search for the Standard Model Higgs Boson with the ATLAS detector at the LHC. *Phys. Lett.*, vol. B716, pp. 1–29, 2012. ISSN 0370-2693. <http://dx.doi.org/http://dx.doi.org/10.1016/j.physletb.2012.08.020>.
- [11] CMS Collaboration: Measurement of the elliptic anisotropy of charged particles produced in PbPb collisions at nucleon-nucleon center-of-mass energy = 2.76 TeV. *Phys. Rev.*, vol. C87, p. 014902, 2013. <http://dx.doi.org/10.1103/PhysRevC.87.014902>.
- [12] Evans L., Bryant P.: LHC Machine. *Journal of Instrumentation*, vol. 3(08), p. S08001, 2008. <http://stacks.iop.org/1748-0221/3/i=08/a=S08001>.
- [13] Huovinen P., Kolb P., Heinz U. W., Ruuskanen P., Voloshin S.: Radial and elliptic flow at RHIC: Further predictions. *Phys. Lett.*, vol. B503, pp. 58–64, 2001. [http://dx.doi.org/10.1016/S0370-2693\(01\)00219-2](http://dx.doi.org/10.1016/S0370-2693(01)00219-2).
- [14] Kovtun P. K., Son D. T., Starinets A. O.: Viscosity in Strongly Interacting Quantum Field Theories from Black Hole Physics. *Phys. Rev. Lett.*, vol. 94, p. 111601, 2005. <http://dx.doi.org/10.1103/PhysRevLett.94.111601>.
- [15] Lunin O., Mathur S.D.: Statistical interpretation of Bekenstein entropy for systems with a stretched horizon. *Phys. Rev. Lett.*, vol. 88, p. 211303, 2002. <http://dx.doi.org/10.1103/PhysRevLett.88.211303>.
- [16] Luzum M.: Flow fluctuations and long-range correlations: elliptic flow and beyond. *J. Phys.*, vol. G38, p. 124026, 2011. <http://dx.doi.org/10.1088/0954-3899/38/12/124026>.
- [17] Luzum M., Ollitrault J.Y.: Eliminating experimental bias in anisotropic-flow measurements of high-energy nuclear collisions. *Phys. Rev.*, vol. C87, p. 044907, 2013. <http://dx.doi.org/10.1103/PhysRevC.87.044907>.
- [18] Maeno T.: PanDA: distributed production and distributed analysis system for ATLAS. *Journal of Physics: Conference Series*, vol. 119(6), p. 062036, 2008. <http://stacks.iop.org/1742-6596/119/i=6/a=062036>.

- [19] Muño P. C., the Atlas Collaboration: Overview of Recent ATLAS Physics Results. *Journal of Physics: Conference Series*, vol. 447(1), p. 012014, 2013. <http://stacks.iop.org/1742-6596/447/i=1/a=012014>.
- [20] Poskanzer A. M., Voloshin S. A.: Methods for analyzing anisotropic flow in relativistic nuclear collisions. *Phys. Rev.*, vol. C58, pp. 1671–1678, 1998. <http://dx.doi.org/10.1103/PhysRevC.58.1671>.
- [21] Qin G. Y., Petersen H., Bass S. A., Müller B.: Translation of collision geometry fluctuations into momentum anisotropies in relativistic heavy-ion collisions. *Phys. Rev. C*, vol. 82, p. 064903, 2010. <http://dx.doi.org/10.1103/PhysRevC.82.064903>.
- [22] Qiu Z., Heinz U. W.: Event-by-event shape and flow fluctuations of relativistic heavy-ion collision fireballs. *Phys. Rev.*, vol. C84, p. 024911, 2011. <http://dx.doi.org/10.1103/PhysRevC.84.024911>.
- [23] Romatschke P.: New Developments in Relativistic Viscous Hydrodynamics. *Int. J. Mod. Phys.*, vol. E19, pp. 1–53, 2010. <http://dx.doi.org/10.1142/S0218301310014613>.
- [24] Schenke B., Jeon S., Gale C.: Anisotropic flow in $\sqrt{s} = 2.76$ TeV Pb+Pb collisions at the LHC. *Phys. Lett.*, vol. B702, pp. 59–63, 2011. <http://dx.doi.org/10.1016/j.physletb.2011.06.065>.
- [25] Snellings R.: Anisotropic flow from RHIC to the LHC. *Eur. Phys. J.*, vol. C49, pp. 87–90, 2007. <http://dx.doi.org/10.1140/epjc/s10052-006-0107-4>.
- [26] Song H.: Hydrodynamic Modeling and the QGP Shear Viscosity. *Eur. Phys. J.*, vol. A48, p. 163, 2012. <http://dx.doi.org/10.1140/epja/i2012-12163-9>.
- [27] STAR Collaboration: Elliptic flow from two and four particle correlations in Au+Au collisions at $\sqrt{s_{NN}} = 130$ GeV. *Phys. Rev.*, vol. C66, p. 034904, 2002. <http://dx.doi.org/10.1103/PhysRevC.66.034904>.
- [28] Steinberg P.: What have we learned about the Quark-Gluon Plasma with the ATLAS detector at the LHC? *Nucl. Phys.*, vol. A, 2014.
- [29] Voloshin S., Zhang Y.: Flow study in relativistic nuclear collisions by Fourier expansion of azimuthal particle distributions. *Zeitschrift für Physik C Particles and Fields*, vol. 70(4), pp. 665–671, 1996. ISSN 0170-9739. <http://dx.doi.org/10.1007/s002880050141>.
- [30] Voloshin S. A., Poskanzer A. M., Snellings R.: *Collective Phenomena in Non-Central Nuclear Collisions, Landolt-Börnstein – Group I Elementary Particles, Nuclei and Atoms*, vol. 23. Springer, Berlin Heidelberg, 2010. ISBN 978-3-642-01538-0. http://dx.doi.org/10.1007/978-3-642-01539-7_10.

Affiliations**Klaudia Burka**

AGH University of Science and Technology, Krakow, Poland, Klaudia.Burka@cern.ch,
<http://www.agh.edu.pl>

Tomasz Bold

AGH University of Science and Technology, Krakow, Poland, Tomasz.Bold@cern.ch,
<http://www.agh.edu.pl>

Iwona Grabowska-Bold

AGH University of Science and Technology, Krakow, Poland, Iwona.Grabowska@cern.ch,
<http://www.agh.edu.pl>

Received: 5.07.2014

Revised: 10.12.2014

Accepted: 11.12.2014